SINTEF
PROCEEDINGS 6

14th International Conference on CFD in
Oil & Gas, Metallurgical and Process Industries
SINTEF, Trondheim, Norway, October 12–14, 2020

# Proceedings from the 14th International Conference on CFD in Oil & Gas, Metallurgical and Process Industries

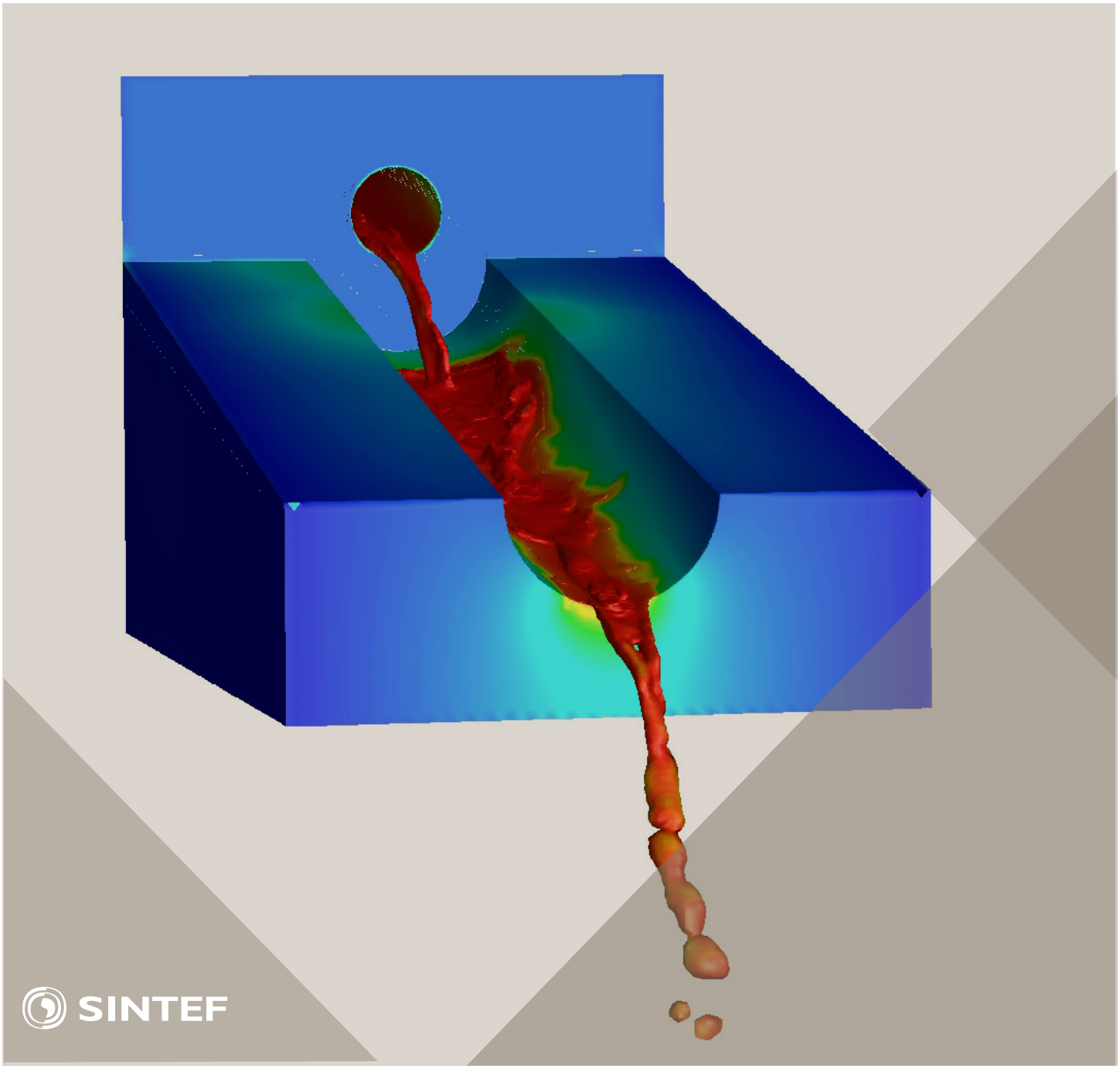

SINTEF Proceedings

Editors:
Jan Erik Olsen, Jan Hendrik Cloete and Stein Tore Johansen

# Proceedings from the 14th International Conference on CFD in Oil & Gas, Metallurgical and Process Industries

SINTEF, Trondheim, Norway
October 12–14, 2020

SINTEF Academic Press

SINTEF Proceedings 6
Editors: Jan Erik Olsen, Jan Hendrik Cloete and Stein Tore Johansen

Proceedings from the 14th International Conference on CFD in Oil & Gas, Metallurgical and Process Industries, SINTEF, Trondheim, Norway, October 12–14, 2020

Keywords:
CFD, fluid dynamics, modelling

Cover illustration: Tapping of metal by Jan Erik Olsen

ISSN 2387-4295 (online)
ISBN 978-82-536-1684-1 (pdf)



SINTEF Academic Press
Address: Børrestuveien 3
PO Box 124 Blindern
N-0314 OSLO
Tel: +47 40 00 51 00

www.sintef.no/community
www.sintefbok.no

# MODELING A TWO-PHASE FLOW IN A DEVICE TO REDUCE THE MUSCLE TONE OF THE HANDS

**Lenar Akhmetshin [1]*, Andrei Chernyshev[1]†**

[1] Bauman Moscow State Technical University, 105005, Moscow, Russia

* E-mail: lenar_akhmetshin_94@mail.ru
† E-mail: av-chernyshev@yandex.ru

## ABSTRACT

In this work, a new design of internal channels for a pneumatic mechanical device was proposed to reduce the muscle tone of the hands. The new design uses a two-phase gas-liquid system as a working medium. Numerical modeling was performed, according to the results of which a cumulative distribution of the average diameter of gas bubbles was obtained at different pressure values in the channels. We used the Euler-Euler approach to simulate a two-phase system, the Reynolds Stress turbulence model and the Population Balance model, which is a set of partial differential integral differential equations that allow performing an average behavior analysis for a set of particles based on an analysis of the behavior of a single particle in local conditions. Simulations have been carried out for different bubble breakup and coalescence models. Graphs of the Sauter bubble diameter has been obtained. The results are to be validated with experimental data in the near future.

**Keywords:** Actuator, manipulator, CFD, two-phase gas-liquid flow, bubble flow.

## NOMENCLATURE

*Greek Symbols*

$\rho$ Mass density, [kg/m$^3$].

*Latin Symbols*

$p$ Pressure, [Pa].

$\mathbf{u}$ Velocity, [m/s].

*Sub/superscripts*

$i$ Index *i.*

## INTRODUCTION

Damage to the vessels of the brain leads to the development of a disease called a stroke or cerebral infarction. Most often, an acute violation of cerebral circulation can be of the ischemic type, when there is a sharp spasm of cerebral vessels with blood clots, leading to the death of brain cells. If a vessel ruptures, then a hemorrhagic stroke develops, accompanied by the formation of a hemorrhage.

Depending on the location of the stroke, the corresponding clinical signs develop. When the motor cortex is damaged, paresis (paralysis) of the upper or lower extremities develop. Most often, unilateral damage occurs: left-sided damage with damage to the right half of the brain, right-sided with damage to the vessels of the left half of the brain [1].

When examining such a patient, there is a restriction or absence of movement in the arm or leg. The appearance of a pronounced muscle spasm, leading to the development of joint contractures, is noted, as well as a loss of sensitivity of certain areas of the skin [2].

The treatment of the stroke itself takes place in a hospital setting. Active vascular and metabolic therapy is performed and takes several weeks, but the restoration of lost functions can take months or years.

The main rehabilitation methods for treating paresis and paralysis are methods of physical education, massage, physiotherapy [3]. The patient himself can engage in physiotherapy exercises, but most often the presence of pronounced contractures and weakness interfere with full-fledged exercises.

A breakthrough in the treatment of such patients was the invention of special electrically driven simulators, which make it possible to perform the necessary movements in a given amplitude and intensity.

We considered the advantages and disadvantages in more detail in our previous work [4]. This work is a continuation of the previous one, where, on the basis of the experiments carried out, a solution was chosen – to create a new structure and use a two-phase gas-liquid system as a working fluid. The main advantage of using such a system is to add additional rigidity to the structure, since the pneumatic manipulator in the previous work [4] did not fully fulfill its functions.

## MATHEMATICAL MODEL

Having reviewed the existing equipment, having considered all the advantages and disadvantages of the designs of elastomeric manipulators, a diagram of a device with branching internal channels is proposed on Figure 1, in which a two-phase medium is used as a working medium: gas-liquid.

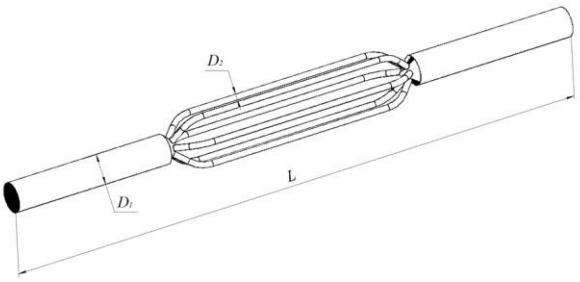


**Figure 1:** Elastomer manipulator internal channels design.

When the pressure inside the channels changes, the volume of gas bubbles changes, which can cause deformation of the wall material and set the structure in motion. In order to prevent the internal channels from "collapsing", they are completely filled with liquid. Due to the branched channels and changes in the volume of gas bubbles in them, an axisymmetric deformation of the elastomeric manipulator actuator occurs. In order to proceed to modeling the deformation and calculating the force created by the actuator, it is necessary to develop an integrated computational pneumo-hydrodynamic model for horizontal two-phase flows in channels. Modeling a two-phase system is not a trivial task. There are various studies concerning the local distribution of the gas volume fraction and the fluid velocity field in horizontal two-phase flows in channels.

The most interesting are dispersed bubbly flow and buoyant bubbly flow since they are able to provide large interfacial regions for heat and mass transfer in general. In fact, there is a big difference between scattered and buoyant bubble flows. It consists in characterizing the role of buoyancy. In a dispersed bubble flow, buoyancy can be neglected in comparison with the effect of the liquid on the gas phase. In a scattered flow, bubbles move in horizontal tubes with some symmetry about the channel axis. However, in the buoyant bubble mode, buoyancy plays an important role, and the bubble concentration in this mode is asymmetric with respect to the channel axis. Due to the buoyancy effect, bubbles move from the bottom to the top of the channel. Similar studies have already been carried out in many works [5-7], experiments were carried out, and models were described, but for each specific case. It is this mode that is subject to mathematical modeling in this work. The goal of this work is to carry out a numerical simulation of a two-phase gas-liquid system inside three-dimensional channels and obtain complete information about three-dimensional fields in terms of the volume average velocities and volume fraction of the dispersed phase.

The volume-averaged velocity fields are significantly influenced by turbulence, and therefore, it is equally important to know the spatial distribution of turbulent kinetic energy and energy dissipation rates, although they are more difficult to measure experimentally, especially in multiphase flow situations.

The numerical calculations obtained in this work are based on the Euler-Euler two-phase model. This model is based on the combined averaged mass and momentum transfer equations for each phase.

The volume fraction of phase *i* is calculated from the continuity equation [8]:

$$\frac{\partial}{\partial t}(\alpha_i \rho_i) + \nabla \cdot (\alpha_i \rho_i \vec{u}_l) = 0 \quad (1)$$

where $\alpha$ is the void fraction, $u$ is the superficial velocity.

The momentum balance for phase *i* [8]:

$$\frac{\partial}{\partial t}(\alpha_i \rho_i \vec{u}_l) + \nabla \cdot (\alpha_i \rho_i \vec{u}_l \vec{u}_l) = \\ = -\alpha_i \nabla p + \nabla \cdot [\alpha_i (\tau_i + \tau_i^t)] + \\ + \alpha_i \rho_i \vec{g} + M_i \quad (2)$$

$$\sum M_i = 0 \quad (3)$$

where $\tau$ is the molecular stress, $\tau^t$ is the turbulent stress, $M_i$ is the momentum transfer in the interface, $\vec{g}$ is the acceleration due to gravity.

Figure 2 shows a diagram of the forces acting on the bubble.

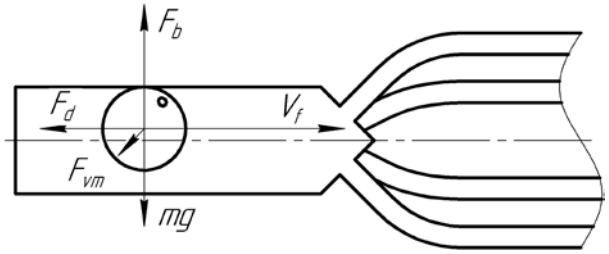


**Figure 2:** Diagram of the forces acting on the bubble.

The total interfacial force acting between the two phases can result from several independent physical effects:

$$\vec{F} = \vec{F}_d + \vec{F}_L + \vec{F}_{VM} + \vec{F}_b + \vec{F}_{TD} + m\vec{g} \quad (4)$$

The forces indicated above are: the drag force $F_d$, $F_b$ is the buoyant force, the lift force $F_L$, the virtual mass force $F_{VM}$, the wall lubrication force $F_{WL}$ and the turbulent dispersion force $F_{TD}$. To simplify our model and calculation, we will not take into account the virtual mass force for now.

## MODEL DESCRIPTION

The breakup of bubbles in turbulent dispersion flows, the Luo and Svendsen model [9] and Lehr model [10] developed by the respective authors, is used. Different models were taken in order to determine how different the results would be and which model to use in subsequent simulations after validation with experiments.

The coalescence model used for modeling, Prince and Blanch [11], was inserted into the software ANSYS Fluent using a user-defined function (UDF) [12].

The Ishii-Zuber drag model was used as a drag force model [13]. The turbulent dispersion force was obtained using the Lopez de Bertodano model [14]. The Antal et al. [15] model was used as a wall lubrication model.

In this work, we used the Reynolds Stress turbulence model (RSM). Population Balance model has been used [16]. This model makes it possible to obtain the distribution of the dispersed phase over the average diameters, which is obtained in the case of formation, coalescence, destruction and disappearance of the gaseous phase.

Numerical modeling was carried out in three-dimensional horizontal channels with diameters $D_1$ = 5 *mm* and $D_2$ = 1 *mm*, channel length $L$ = 100 *mm* (Figure 1). The calculations were carried out using ANSYS Fluent software. The flow of glycerine was considered as the continuous liquid phase, while the air was taken as the dispersed gas phase. The interfacial tension was assumed to be $\gamma = 0.07\ N/m$. The sizes of gas bubbles were set in the range from 0.1 mm to 0.9 *mm*. This range has been subdivided into ten discrete bubble sizes.

The structured mesh in each block is generated using commonly curved coordinates to accurately represent flow boundaries. To select a mesh size, the effect of changing its shape and size was investigated. Several simulations were carried out using a different number of a grid: 112843, 879324, 1299505. The grid with the largest number of cells showed the best convergence. As a result, a grid with the number of cells 1299505 was chosen (Figure 3). The calculations were carried out at the university workstation.

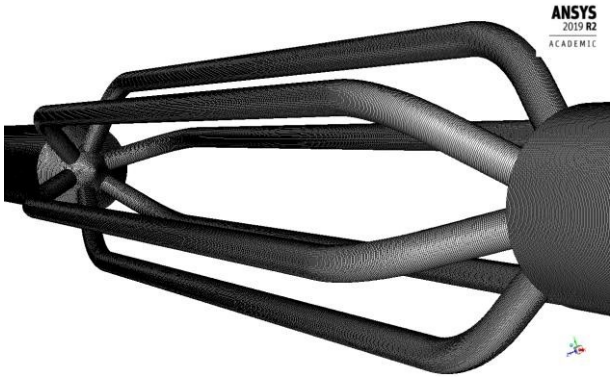


**Figure 3:** Hexahedral structured mesh selected for the calculation number of cells 1299505.

For calculations, time step 0.01 *s* was used. The Phase Coupled SIMPLE scheme was used. Under-relaxation factors were used. At the pipe inlet, uniform gas and liquid velocities and volume fractions have been specified. At the channel outlet, a relative average static pressure of zero was specified.

## RESULTS

Simulations were carried out under fully developed bubble flow conditions for the air-glycerine system. The velocity of liquid ($v_g$) and gas ($v_l$) is equal to $U_{mean}$ = 0.5 *m/s*, and the average volumetric gas fraction $\varphi$ = 30%. The simulation results are the cumulative distribution at the outlet of the channels $D_1 = 5\ mm$, $D_2 = 1\ mm$, respectively (Figure 4). The graph shows that there is a high probability of the presence of air bubbles with a size of ≈ 0.7 *mm*, and it is ≈ 80%.

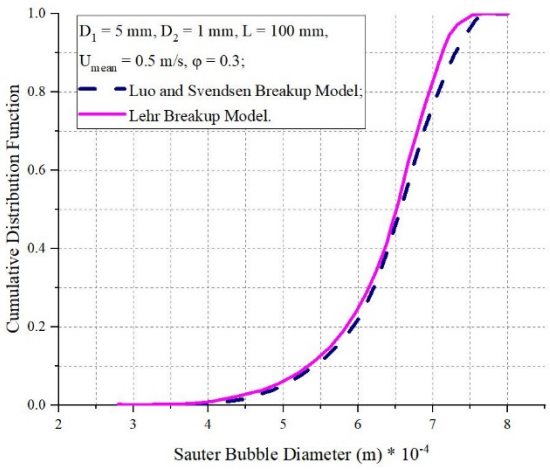


**Figure 4:** Cumulative Bubble distribution function.

Figures 5-6 show the distributions of bubble concentration along the diameter for different tube diameters for $D_1$ = 5 *mm*, and $D_2$ = 1 *mm*.

It should be noted that both models give approximately the same result and do not differ much from each other. It should be concluded that further modeling can use one of these models. When using the Luo and Svendsen [9] breakup model, the convergence of the calculation was carried out faster.

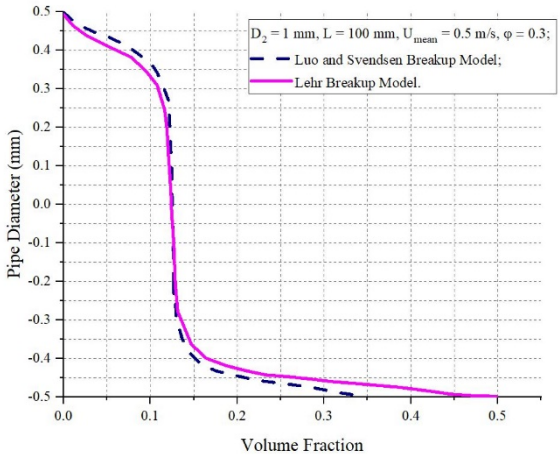


**Figure 5:** Bubble Volume Concentration Distribution across Pipe Diameter.

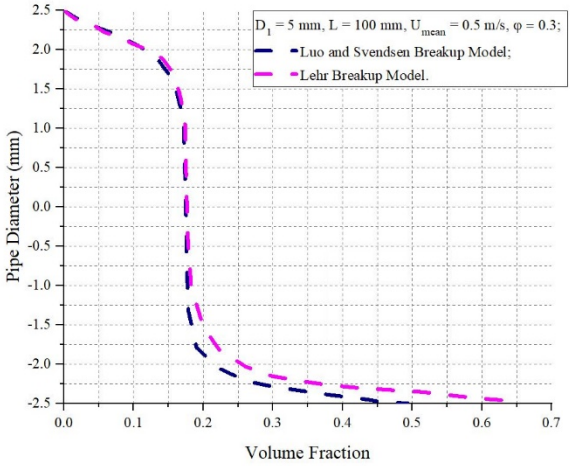


**Figure 6:** Bubble Volume Concentration Distribution across Pipe Diameter.

Analyzing the graphs, it can be seen that bubbles of large diameters accumulate mainly in the channel with a diameter $D_1 = 5\ mm$.
At the inlet to thin channels with a diameter of $D_2 = 1\ mm$, bubbles are evenly distributed. The main concentration of the gas phase is located in the upper part of the channels, which is explained by the action of the gravitational component. Figure 7 shows the results of the bubble diameter distribution. The scale shows data on bubble diameters $d_b, m$.

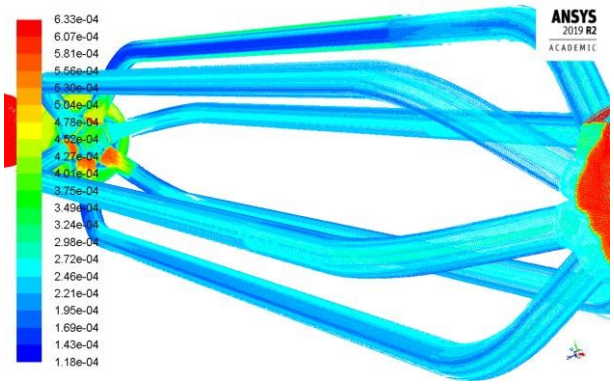


**Figure 7:** Dispersed phase distribution within the channel, the scale shows the values of the bubble diameters $d_b, m$.

Thus, we have obtained data in what places of the channel and what sizes of bubbles can be obtained with a given geometry of the channels. The accuracy of the calculated data will be evaluated by experiments in future work.

## CONCLUSION

A comprehensive computational pneumo-hydrodynamic model for horizontal two-phase flows in channels has been developed. From the calculated data, a distribution of the dispersed gas phase inside the channel, and cumulative distribution over the diameters of air bubbles, were obtained. Thus, using the developed pneumo-hydrodynamic model, we can predict where in the channel and what size bubbles are formed in the gas-liquid system. This enables the modeling of the deformation and calculation of the forces created by the actuator of the elastomeric manipulator. Calculations were carried out for two different breakup models Luo and Svendsen [9] and Lehr model [10], using a user-defined function in ANSYS Fluent (2019). And a coalescence model was introduced. Data were obtained on the distribution of the Sauter bubble diameter over the entire tubing system and the distribution of the volume concentration of bubbles for different diameters. In the future, it is planned to conduct an experiment and compare the simulated data with the experimental ones. Based on the validation, future decisions creating a hand rehabilitation device.

## REFERENCES

[1] B. Peele, T. Wallin, H. Zhao and R. Shepherd, “3D printing antagonistic systems of artificial muscle using projection stereolithography”, Bioinspiration & Biomimetics, 10 (5) (2015), 567-943;

[2] B. Homberg, R. Katzschmann, M. Dogar and D. Rus, “Haptic Identification of Objects using a Modular Soft Robotic Gripper”, Intelligent Robots and Systems (IROS), (2015) IEEE/RSJ International Conference on. IEEE;

[3] R. Deimel and O. Brock, “A compliant hand based on a novel pneumatic actuator,” Robotics and Automation (ICRA), 2013 IEEE International Conference on. IEEE, (2013), 2047-2053;

[4] Meretskaya, E.R., Chernyshev, A.V. “Calculating and theoretical research and determination of the functional parameters of a pneumo-mechanical device actuator”, (2018) AIP Conference Proceedings, № 030045;

[5] A. J. Ghajar and C. C. Tang, “Advances in Void Fraction”, Flow Pattern Maps and Non-Boiling Heat Transfer Two-Phase Flow in Pipes with Various Inclinations, vol. 1. (2009);

[6] R. Brito, “Effect of Medium Oil Viscosity on Two-Phase Oil-Gas Flow Behavior in Horizontal Pipes”, The University of Tulsa, (2012);

[7] H. Matsubara and K. Naito, “Effect of liquid viscosity on flow patterns of gas-liquid two-phase flow in a horizontal pipe”, Int. J. Multiph. Flow, 37 (10) (2011), 1277–1281;

[8] Esteban Guerrero, Felipe Muñoz and Nicolás Ratkovich, “Comparison between Eulerian and VOF Models for two-phase flow assessment in vertical pipes”, CT&F, 7 (1) (2017) 73 – 84;

[9] H. Luo, H. Svendsen, “Theoretical model for drop and bubble breakup in turbulent dispersions”, AIChE J. 42 (1996);

[10]F. Lehr, D. Mewes, M. Millies, Bubble-Size Distribution and Flow Fields in Bubble Columns, AIChE Journal 48(11) (2002) 2426 – 2443;

[11] M.J. Prince, H.W. Blanch, “Bubble coalescence and breakup in air sparged bubble columns”, AIChE J. 36 (1990) 1485–1499;

[12] ANSYS Fluent Theory Guide, ANSYS Fluent Release 15.0: ANSYS (Europe Ltd, 2013) 42 p.;

[13] M. Ishii, N. Zuber, “Drag coefficient and relative velocity in bubble, droplet or particulate flows”, AIChE J. 25 (1979) 843–855;

[14] M.A. Lopez de Bertodano, “Turbulent bubbly two-phase flow in a triangular duct”, Ph.D. dissertation, Rensselaer Polytechnic Institute, 1992;

[15] S.P. Antal, R.T. Lahey, J.E. Flaherty, “Analysis of phase distribution in fully-developed laminar bubbly two phase flow”, Int. J. Multiphase Flow 7 (1991) 635;

[16] Nopens, I., Torfs, E., Ducoste, J., Vanrolleghem, P.A., Gernaey K.V., 2014, “Population balance models: a useful complementary modelling framework for future WWTP modelling”, Water Sci. Technol. 71(2), 159-167.